A Novel Method To Synthesize Amorphous Silica−Alumina Materials with Mesoporous Distribution without Using Templates and Pore-Regulating Agents

ARTICLE *in* CHEMISTRY OF MATERIALS · JANUARY 2002

Impact Factor: 8.35 · DOI: 10.1021/cm010270w

A Novel Method To Synthesize Amorphous Silica−Alumina Materials with Mesoporous Distribution without Using Templates and Pore-Regulating Agents

Nan Yao,[†] Guoxing Xiong,*[,†] Mingyuan He,[‡] Shishan Sheng,[†] Weishen Yang,[†] and Xinhe Bao[†]

State Key Laboratory of Catalysis, Dalian Institute of Chemical Physics, Chinese Academy of Sciences, P.O. Box 110, Dalian 116023, People's Republic of China, and Research Institute of Petroleum Processing, SINOPEC, Beijing 100083, People's Republic of China

Received March 28, 2001. Revised Manuscript Received August 27, 2001

In this study, a novel sol−gel method is used to synthesize amorphous silica−alumina materials with a narrow mesoporous distribution and various Si/Al molar ratios without using any templates and pore-regulating agents. During the preparation procedure, only inexpensive inorganic salts were used as raw materials, instead of expensive and harmful alkoxides. The precursor sol was dried at room temperature in a vacuum box kept at 60 mmHg until it began to form the gel. The results of a nitrogen sorption experiment indicate that the synthesized materials with different Si/Al molar ratios have similar mesoporous distributions (within 2−12 nm). Moreover, it was found that the material's pore size distribution remains at a similar value during the heat treatment from room temperature to 550 °C. On the basis of the nitrogen sorption, TEM, and AFM characterization results, a formation mechanism of mesopores which accounts for the experimental data is also suggested. This suggested mechanism involves rearrangement of the primary particles during the drying process to form the precursors of the similarly sized mesopores. The synthesized materials were characterized by XRD, thermal analysis (TG/DTA), ^{27}Al and ^{29}Si MAS NMR spectroscopy, SEM, TEM, and AFM. The results of ^{27}Al and ^{29}Si MAS NMR indicate that the distribution of silicon and aluminum in the synthesized materials is more uniform and homogeneous than that in the mixed oxides prepared via the traditional sol−gel method even at high alumina contents. The type and density of the acid sites were studied using pyridine adsorption−desorption FTIR spectroscopy. It was shown that the acidity of the synthesized materials is higher than that of the silica−alumina materials prepared by conventional methods.

1. Introduction

Most shape-selective reactions utilized by industry involve catalysts having pore diameters between 0.5 and 0.6 nm. This size is sufficient to accommodate a broad spectrum of small molecules of technological interest. However, the application of heterogeneous catalysts in processing large molecules, which are of increasing importance, is limited by the pore size of the microporous zeolite used and/or by the pore geometry of the support. Thus, the demand for mesoporous materials has triggered major efforts in academic and industrial laboratories.[1]

Since the discovery of M41-S molecular sieves in 1992 by Mobile scientists,[2] many types of aluminosilicate materials such as FSM-16,[3] HMS,[4] SBA,[5] MSU,[6] KIT-1,[7] MSA,[8] and ERS-8[9] with a narrow pore size distribution in the range 1−10 nm have been described. All of these aluminosilicates show an ordered pore structure (i.e., narrow pore size distribution in the micro-mesopore region), while being amorphous materials.

As a general rule, amorphous materials with ordered pore structure are obtained by using various types of templates and pore-regulating agents (PRAs), which can give rise to the formation of micelles (e.g., for MCM-41, FSM-16, and HMS syntheses) or clusters (e.g., for MSA and ERS-8 syntheses). Moreover, all these aluminosilicates are mainly high-silica materials ($SiO_2/Al_2O_3 > 10$). The properties of the surfactant and PRA as well as the synthetic conditions can affect the physical and chemical

* To whom correspondence should be addressed. Fax: +86-411-4694447. E-mail: gxxiong@ms.dicp.ac.cn.
[†] Chinese Academy of Sciences.
[‡] SINOPEC.

(1) Biz, S.; Occelli, M. L. *Catal. Rev.−Sci. Eng.* **1998**, *40* (3), 330.
(2) Beck, J. S.; Vartuli, J. C.; Roth, W. J.; Leonoswicz, M. E.; Kresge, C. T.; Schmitt, K. D.; Chu, C. T.-W.; Olson, D. H.; Sheppard, E. W.; McCullen, S. B.; Higgins, J. B.; Schlenker, J. L. *J. Am. Chem. Soc.* **1992**, *114*, 10834.
(3) Inagaki, S.; Fukushima, Y.; Kuroda, K. *J. Chem. Soc., Chem. Commun.* **1993**, 680.
(4) Tuel, A.; Gontier, S. *Chem. Mater.* **1996**, *8*, 114.
(5) Huo, Q.; Margolese, D. I.; Stucky, G. D. *Chem. Mater.* **1996**, *8*, 1147.
(6) Bagshaw, S. A.; Prouzet, E.; Pinnavaia, T. J. *Science* **1995**, *269*, 1242.
(7) Ryoo, R.; Kim, J. M.; Shin, C. H.; Lee; J. Y. *Stud. Surf. Sci. Catal.* **1997**, *105*, 45.
(8) Bellussi, G.; Perego, C.; Carati, A.; Peratello, S.; Previde Massara, E.; Perego, G. *Stud. Surf. Sci. Catal.* **1994**, *84*, 85.
(9) Perego, G.; Millini, R.; Perego, C.; Carati, A.; Pazzuconi, G.; Bellussi, G. *Stud. Surf. Sci. Catal.* **1997**, *105*, 205.

10.1021/cm010270w CCC: $22.00
Published on Web 12/01/2001

properties of the final product. For example, Manton et al. found the pore size and its distribution in the calcined solids changed with the type of tetraalkylammonium cations used in the synthesis.[10] Snel showed that the syneresis process, the pH value, the concentration of reactants, and the PRA could all be used to control the porous structure. By selecting an appropriate PRA, one could achieve the desired mean pore size in the range 7.5−40 nm.[11−13] The work of Bellussi and Perego et al. showed that the volume fraction of NR_4^+ rather than the length of the R alkyl chain determines the formation of microporous (ERS-8) or mesoporous silica−alumina materials.[9]

It is clear that all the above synthesis methods use templates or PRAs. As far as we know, no one has described the synthesis of mesoporous materials with a controlled pore size distribution other than by using templates and PRAs. In addition, the raw materials usually used in the preparation of silica−alumina materials were alkoxides.[14] It is well-known that the disadvantages of using alkoxides include the high cost, health hazards of organic solutions, pollution, and so on.

In this paper, we present a novel sol−gel method to synthesize amorphous silica−alumina materials with mesoporous distribution and a low Si/Al molar ratio (SiO_2/Al_2O_3 < 10) without using any pore-regulating reagents and templates. During the whole experiment, we used inexpensive inorganic salts as raw materials instead of expensive alkoxides. At the same time, we also examined the influence of the Si/Al molar ratio on the physicochemical properties of the synthesized materials.

2. Experimental Section

2.1. Materials Preparation. All chemicals used were AR grade, and the water was deionized and twice distilled. A 0.96 M aluminum nitrate solution was added dropwise to a 50 mL water glass solution (SiO_2, 0.39 mol/L; Na_2O, 0.125 mol/L) under vigorous stirring until the desired Si/Al molar ratio was attained. A precipitate was formed after the addition of the aluminum nitrate solution. An appropriate amount of 2.5% ammonium hydroxide was then added to bring the pH to about 8.0. The precipitate was collected by centrifugation and washed seven times to remove the sodium ions. The first and the last two washing cycles used water, and the rest used a 70 mL NH_4NO_3 (1.2 M) solution. After washing, the precipitate was put into 200 mL of water and the resulting mixture stirred for 0.5 h to form a suspension. Then a certain quantity of 0.94 M nitric acid, depending on the Si/Al molar ratio, was added to the suspension to obtain the sol sample. The pH values of stable sols with different Si/Al molar ratios are reported in Table 1.

After being stirred for 12 h, the sol was dried at room temperature in a vacuum box kept at 60 mmHg until it began to form the gel sample. The drying process is described in detail below. A plate of silica gel spheres and the sol samples were put together in a vacuum box. The box was evacuated to obtain the vacuum value of 60 mmHg. After this vacuum was attained, the valve connecting the pump and the vacuum box was closed. When silica gel spheres were saturated with adsorbed water, the valve was opened and another plate of silica gel spheres was put into the box. The box was evacuated to obtain the same vacuum, and the valve was closed again. This step was repeated until the sol began to form the gel. Finally, the gels were calcined in air at 550 °C for 10 h to obtain the solid samples. In this work, the sol and solid samples prepared by this new method are defined as VSG samples.

Table 1. pH Value and Average Particle Diameter of the Precursor Sols

sample no.	Si/Al molar ratio	pH value	avg particle diam (nm)
VSG1	1	3.22	272.5
VSG2	4	2.77	500.4
VSG3	7	2.41	753.6
VSG4	10	2.12	1374.8

An amorphous silica−alumina sample with a Si/Al molar ratio of 1 was also prepared by the conventional cogel method using the same raw materials. During the preparation, the precipitate was also washed seven times. After being dried at 50 °C for 12 h, the gel was calcined at 550 °C in air for 10 h to obtain the solid sample, which is defined as MG.

2.2. Characterization. The pH values were monitored using a Cole-Parmer 5986-50 pH meter. A N_4 plus laser scattering particle meter (Coulter) was used to measure the sol particle diameter distribution at a 90° angle to the light beam. Drops of the sol were diluted in the sample cuvette with water to give the appropriate intensity for measurement.

N_2 adsorption−desorption isotherms of materials at 77 K were obtained by a static volumetric method with an Omnisorp-100CX apparatus from Coulter. The solid samples were first degassed at 350 °C under vacuum (10^{-6} Torr) for at least 3 h before their isotherms were recorded. The specific surface area of the samples was calculated on the basis of the Brunauer, Emmett, and Teller (BET) theory. From the adsorption isotherm, the Barrett, Joyner, and Halenda (BJH) theory was used to calculate the mesopore volume and the mesoporous distribution, and the *t*-plot method was applied to calculate the micropore volume.

Powder XRD characterization was performed with a Rigaku D/MAX-RB using a copper target at 40 kV and 100 mA. Thermogravimetric (TG) and differential thermal (DTA) analyses were done on a Perkin-Elmer TDA-1700 instrument in the temperature range of 40−850 °C with a 25 mg sample. The conditions were heating rate 5 °C/min and air flow 30 cm^3/min.

All NMR spectra were taken on a DRX400 nuclear magnetic resonance spectrometer from Bruker. The chemical shifts of aluminum and silicon were referenced to 1 M $Al_2(SO_4)_3$ solution and DSS (3-(trimethylsilyl)propanesulfonic acid sodium salt), respectively. ^{27}Al NMR spectra of the sol samples were recorded at 104.3 MHz, and ^{29}Si NMR spectra were recorded at 79.49 MHz. All spectra were corrected for background signals arising from aluminum and silicon in the probe, using a blank consisting of D_2O, the spectra of which were recorded under the same conditions as those used for the samples. Solid-state ^{27}Al MAS NMR spectra were run at 104.3 MHz at a spinning rate of 8 kHz, while the solid-state ^{29}Si MAS NMR spectra were run at 79.49 MHz at a spinning rate of 4 kHz.

The nature and strength of the acid sites were studied by monitoring the thermal desorption of chemisorbed pyridine using Fourier transform infrared spectroscopy. Pyridine was strictly dehydrated and was thoroughly degassed by several freeze−pump−thaw cycles prior to its use as a probe. Self-supported wafers (6−8 mg/cm^2) used in the adsorption studies were prepared by pressing samples between 15 mm diameter dies for 2 min at 10 MPa of pressure. The wafers were mounted in homemade in situ quartz IR cells with CaF_2 windows. IR spectra were recorded by using a Nicolet Impact 410 FTIR spectrometer, fully controlled by Nicolet OMNIC software. All the IR spectra were measured in the following conditions: scan 32 times, resolution 4 cm^{-1}, detector DTGS KBr.

Before the pyridine adsorption, the wafers were heated at 400 °C for 2 h in a vacuum (10^{-2} Pa). A reference spectrum

(10) Manton, M. R. S.; Davidtz, J. C. *J. Catal.* **1979**, *60*, 156.
(11) Snel, R. *Appl. Catal.* **1984**, *12*, 347.
(12) Snel, R. *Appl. Catal.* **1984**, *12*, 189.
(13) Snel, R. *Appl. Catal.* **1984**, *11*, 271.
(14) Pozarnsky, G. A.; McCormick, A. V. *J. Non-Cryst. Solids* **1995**, *190*, 212.

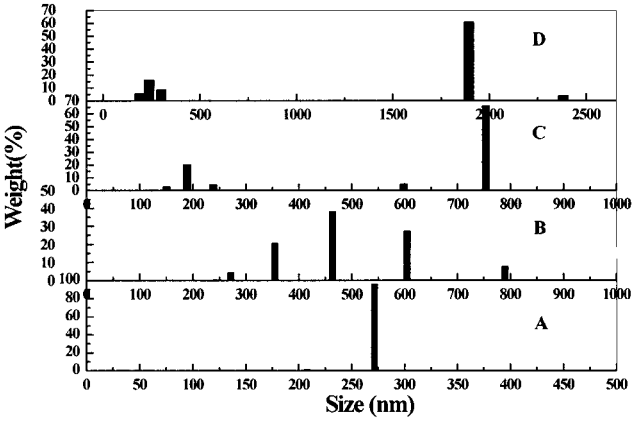

Figure 1. Particle diameter distribution of VSG sol samples with different Si/Al molar ratios measured by a laser light scattering meter: A, VSG1 sol (Si/Al = 1); B, VSG2 sol (Si/Al = 4); C, VSG3 sol (Si/Al = 7); D, VSG4 sol (Si/Al = 10).

was recorded at room temperature. For acidity measurements, 500 Pa of pyridine was introduced into the in situ cell at room temperature. The sample was then degassed at 150 °C for 30 min in a vacuum (10^{-2} Pa) and cooled to room temperature to record the spectrum. This process was repeated for thermal desorption at 250, 350, and 450 °C, respectively. Only the 1700−1400 cm^{-1} part of the IR spectra, obtained by subtracting the absorbance reference spectrum from the absorbance spectra recorded after probe adsorption, was considered in the present work. Pyridine concentrations on Brönsted and Lewis acid sites were inferred from the intensities of the IR bands at about 1546 and 1454 cm^{-1}, respectively, and by using the equations developed by Emeis for porous aluminosilicates.[15]

The scanning micrographs of the synthesized materials were made using a JEM1200EX scanning electron microscope. TEM images were also taken using a JEM1200EX microscope, with an accelerating voltage of 100 kV. AFM images were recorded on a Digital Instruments Nanoscope multimode microscope operating in tapping mode. The sol specimen was diluted to 0.01 M before observation.

3. Results and Discussion

3.1. Properties of the Precursor Sol. Figure 1 shows the particle diameter distribution of the sol samples with different Si/Al molar ratios measured by the laser light scattering meter. It is noteworthy that the particle diameter distribution is narrow when the sample has a low Si/Al molar ratio. However, the particle diameter broadens and, eventually, a bimodal distribution appears as the Si/Al molar ratio is increased.

Table 1 summarizes the effect of the Si/Al molar ratio on the precursor sols. The average particle diameters of the sol samples are large in the range 272.5−1374.8 nm. Increasing the Si/Al molar ratio results in a decrease in the pH value and a drastic increase in the average particle diameter. According to the Derjaguin−Landau−Vervey−Overbeck (DLVO) theory,[16] particle aggregation is due to the reduction in the double-layer repulsion. This phenomenon occurs when the surface potential is decreased by a decrease in the pH value. Therefore, it is reasonable to assume that the average particle diameter increases with a decrease in the pH value. This is due to the fact that a higher degree of aggregation will be attained, which leads to the formation of larger particles, along with a decrease in the pH value.

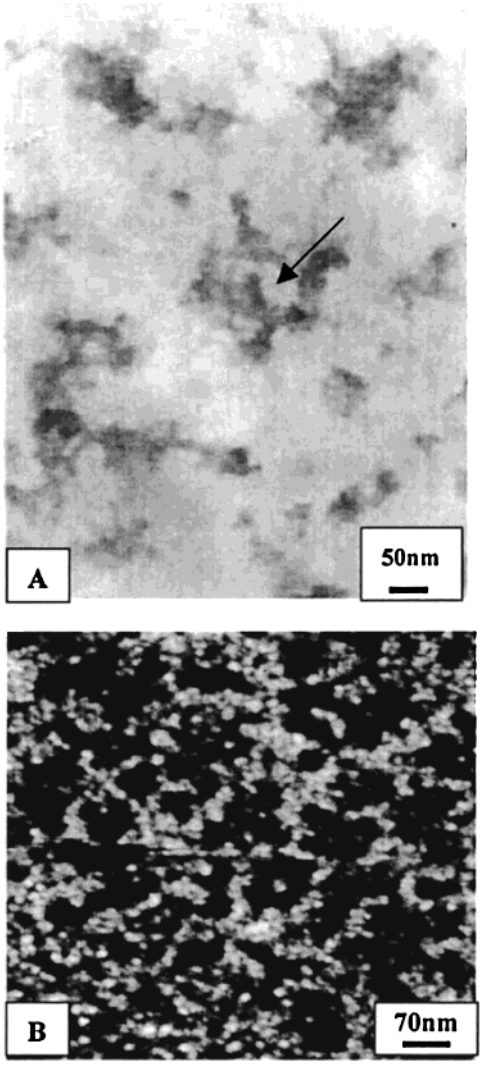

Figure 2. (A) TEM image of the particles in the VSG1 sol sample. The arrow denotes the large fluid-filled interstice existing inside the secondary particles. (B) AFM image of the VSG1 sol sample.

Figure 2 shows the VSG1 sol particle's morphology observed by TEM and AFM. It is seen that the large secondary particles aggregated by spherical primary particles are well dispersed. Furthermore, it is observed from the AFM image that the primary particles have a narrow size distribution within 10−20 nm. When this result is compared with the data shown in Table 1, it is clear that the average particle diameter measured by the laser light scattering meter is the size of the secondary particles.

It is known that Al^{3+} gives aquo cations $[Al(OH_2)_6]^{3+}$ at a low pH level (pH < 3). Condensation can be performed by increasing the pH. At pH > 3, condensation reactions occur with formation of olated polycations.[17] Therefore, ^{27}Al NMR and ^{29}Si NMR spectra of VSG1 (pH > 3) and VSG4 (pH < 3) sol samples were chosen to investigate the Al and Si species.

(15) Emeis, C. A. *J. Catal.* **1993**, *141*, 347.
(16) Brinker, C. J.; Scherer, G. W. *Sol−gel Science the physicals and Chemistry of Sol−gel Processing*; Academic Press Inc.: New York; Harcourt Brace Jovanovich: Orlando, FL, 1990; p 246.
(17) Livage, J. *Stud. Surf. Sci. Catal.* **1994**, *85*, 11.

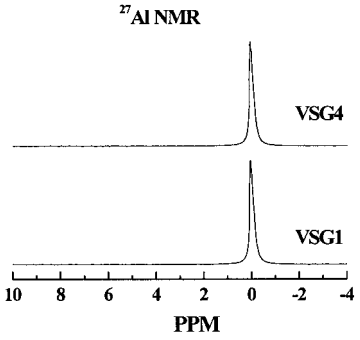

Figure 3. ^{27}Al NMR spectra of the VSG1 and VSG4 sol samples.

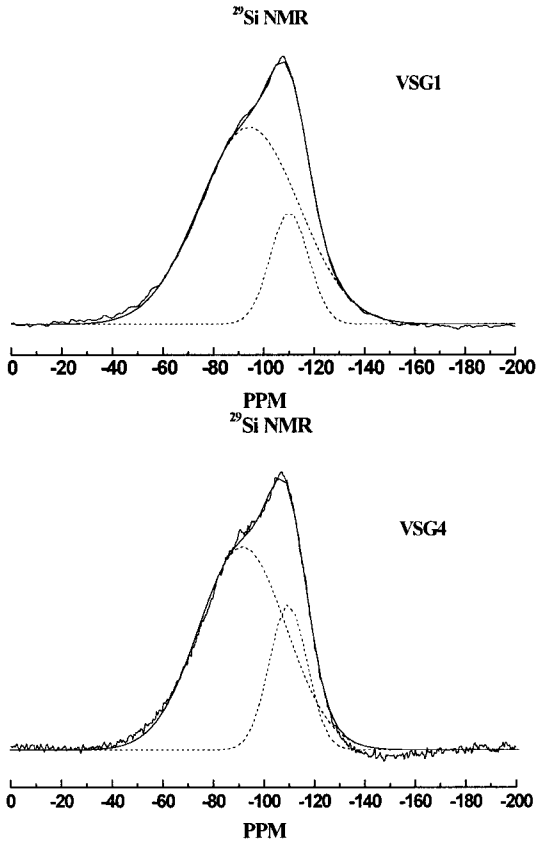

Figure 4. ^{29}Si NMR of the VSG1 (A) and VSG4 (B) sol samples. The dashed lines in the pattern are the results of deconvolution by using the Gauss equation.

Figure 3 displays the ^{27}Al NMR spectra for these sol samples. A sharp peak appears only at 0 ppm, which can be assigned to monomer $Al(H_2O)_6^{3+}$. Therefore, although the pH value of the VSG1 sol sample is above 3.0, the ^{27}Al NMR result still shows that there are unhydrolyzed $Al(H_2O)_6^{3+}$ species. Figure 4 shows the samples' ^{29}Si NMR spectra. Before discussing the results, it is necessary to clarify the notation Q^n often used to denote Si species. The superscript *n* denotes the number of bridging oxygens (−OSi) surrounding the central silicon. As shown in Figure 4, the spectral deconvolutions reveal a resonance at −90 ppm, tentatively assigned to Q^2 [$Si(OSi)_2(OH)_2$] species, and another resonance at −110 ppm assigned to Q^4 [$Si(OSi)_4$] species.[18] Thus, the ^{27}Al and ^{29}Si NMR characterizations show that the precursor sol samples have the same Al and Si species, even though they have different Si/Al molar ratios and pH values.

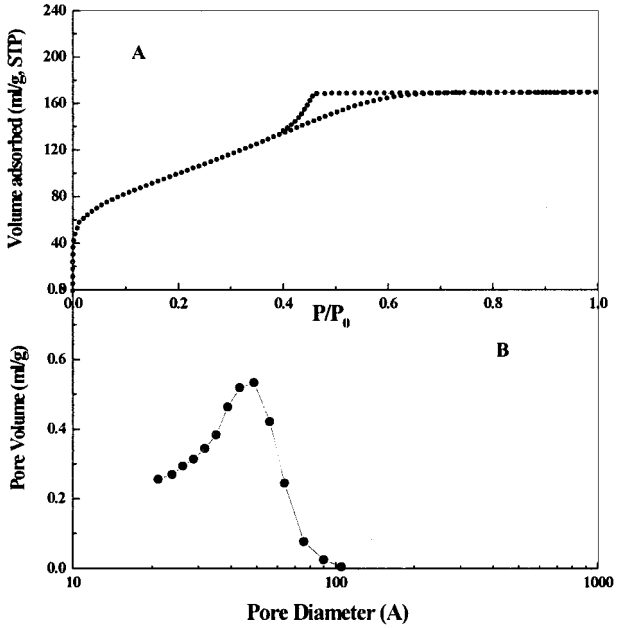

Figure 5. (A) Nitrogen adsorption−desorption isotherm of the VSG1 sample. (B) Pore size distribution of the VSG1 sample.

3.2. Nitrogen Adsorption−Desorption, XRD, and SEM Results. The representative nitrogen adsorption−desorption isotherm of the VSG1 solid sample is presented in Figure 5A. This is a type IV isotherm typical of mesoporous materials. A step at intermediate relative pressures higher than $P/P_0 = 0.4$ indicates capillary condensation within the mesopores. There is no sharp rise in N_2 uptake as the pressure reaches saturation (P/P_0 is near 1), which indicates that no macropores exist in the material.[19] On the other hand, the H2-type hysteresis loop can also be observed in the isotherm. Because of the appearance of the H2-type loop in the desorption branch, it is better to calculate the pore size distribution using the adsorption branch, rather than the desorption branch, by taking into account the recent study.[20] Figure 5B shows the VSG1 solid sample's pore size distribution, for example. It is seen that the sample gives a single maximum in its distribution.

Figure 6A shows the MG sample's nitrogen sorption isotherm for comparison. Although it is also a type IV isotherm, it is very different from that of the VSG materials. Figure 6B displays the MG sample's pore size distribution calculated also from the adsorption branch. It is obvious that the MG sample has a much broader and uncontrolled pore size distribution.

Table 2 shows some physiochemical properties of the solid samples. The VSG materials have high BET surface areas. It was also found that these materials have larger specific surface areas than MG samples. Besides the mesopore volume, the *t*-plot method was also applied to calculate the micropore volume in the materials, because the BJH method can only be used for mesoporous materials. It was seen that very few micropores were detected in some VSG solids. In Table

(18) Brinker, C. J.; Scherer, G. W. *Sol−gel Science the physicals and Chemistry of Sol−gel Processing*; Academic Press Inc.: New York; Harcourt Brace Jovanovich: Orlando, FL, 1990; p 166.
(19) Gregg, S. J.; Sing, K. S. W. *Adsorption, surface area and porosity*, 2nd ed.; Academic Press: New York, 1982.
(20) Rouquerol, F.; Roquerol, J.; Sing, K. S. W. *Adsorption by powders and porous solids*; Academic Press: London, 1999.

Table 2. Physicochemical Characteristics of the Materials

sample no.	Si/Al molar ratio	BET *C* value	MEPV[a] (mL/g)	MIPV[b] (mL/g)	specific surface area (m^2/g)	mean pore size (nm)	pore size distribution (nm)
VSG1	1	69.811	0.216	0.006	366.10	3.84	2.38−10.52
VSG2	4	65.100	0.268	0.000	389.35	3.96	2.11−11.97
VSG3	7	60.434	0.294	0.000	493.89	3.54	2.12−12.08
VSG4	10	63.042	0.244	0.030	542.99	3.28	2.12−10.61
MG	1	87.364	0.663	0.000	301.06	10.28	2.11−66.27

[a] Mesopore volume calculated by the BJH method from the adsorption branch. [b] Micropore volume calculated by the *t*-plot method from the adsorption branch.

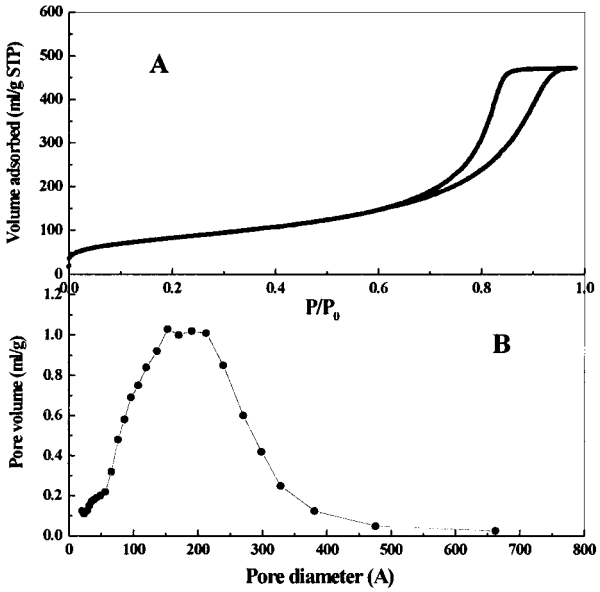

Figure 6. (A) Nitrogen adsorption−desorption isotherm of the MG sample (Si/Al = 1). (B) Pore size distribution of the MG sample.

2, another feature is the pore size distribution. All the VSG materials have similar mean pore sizes and pore size distributions. This property is different from the literature data in which the pore size always changes with the Si/Al molar ratio.[21] In conclusion, the results shown in Figures 5 and 6 and Table 2 imply that, as compared to the conventional method, the developed method can obtain amorphous silica−alumina materials, which have a narrow mesoporous distribution, a larger specific surface area, and various Si/Al molar ratios, without using templates and PRAs.

X-ray analysis (not shown in this paper) reveals that all the solid samples are amorphous. It is interesting to note that however long the maturation period was, the sol samples would not yield crystals. Figure 7 shows the micrograph of the solid sample. Although the solid is not crystalline, the external structure shows well-defined cubes. This result can be explained according to the theory suggested by Zarzycki. When the gel is formed, the particles are not ordered (colloid). But if such a gel is thermally treated, it undergoes microstructural rearrangements when the temperature is higher than the vitrifying point. The molecules are then located in such a way that the net result is a cube.[22]

3.3. Formation Mechanism of the Mesopores in the Solid Samples. After analysis of the data shown

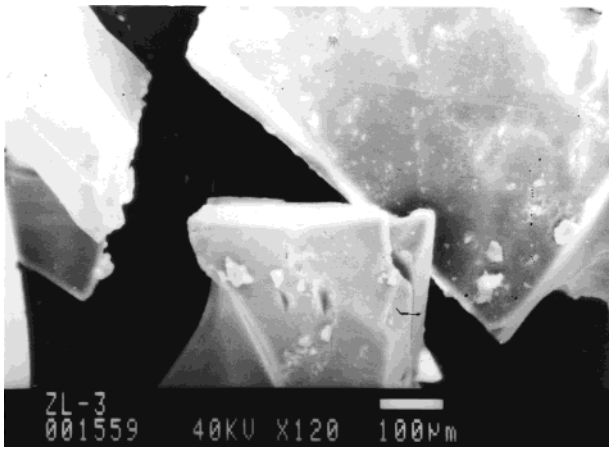

Figure 7. Micrograph of the VSG solid sample.

in Table 1, it is evident that the precursor sol of each sample has large and different average particle diameters. Two things need to be determined: how the small mesopores with a narrow size distribution are formed from these precursor sol particles and why the final materials have similar pore size distributions. In an attempt to provide answers, a formation mechanism of mesopores is proposed on the basis of the TEM, AFM, and N_2 sorption results. When the precursor sol is dried in a vacuum box as the solvent evaporates, these large secondary particles can maintain their original structure and close up gradually until they pack together. During this period, it is reasonable to visualize that fluid-filled interstices of various sizes are formed between secondary particles. Furthermore, there are some large fluid-filled interstices inside secondary particles due to the non-close-packing of primary particles (see Figures 2 and 8).

With further evaporation of the solvent, solid−liquid and solid−vapor interfaces appear. At this time, capillary pressure will appear due to the difference between the solid−vapor and solid−liquid interfacial energies. The magnitude of the capillary pressure experienced by the network depends on the surface tension γ_{LU}, the contact angle θ, and the pore radius r according to eq 1.[23] Thus, when the capillary pressure appears, the

$$P_c = \frac{2\gamma_{LU}\cos(\theta)}{r} \quad (1)$$

liquid will preferentially invade the smaller interstices in which the capillary suction is the greatest; that is,

(21) Witte, Bruno M. De; Uytterhoeven, Jan B. *J. Colloid Interface Sci.* **1996**, *181*, 200.
(22) Zarzycki, J. *J. Non-Cryst. Solids* **1982**, *48*, 105.
(23) Brinker, C. J.; Smith, D. M.; Deshpande, R.; Davis, P. M.; Hietala, S.; Frye, G. C.; Ashley, C. S.; Assink, R. A. *Catal. Today* **1992**, *14*, 155.

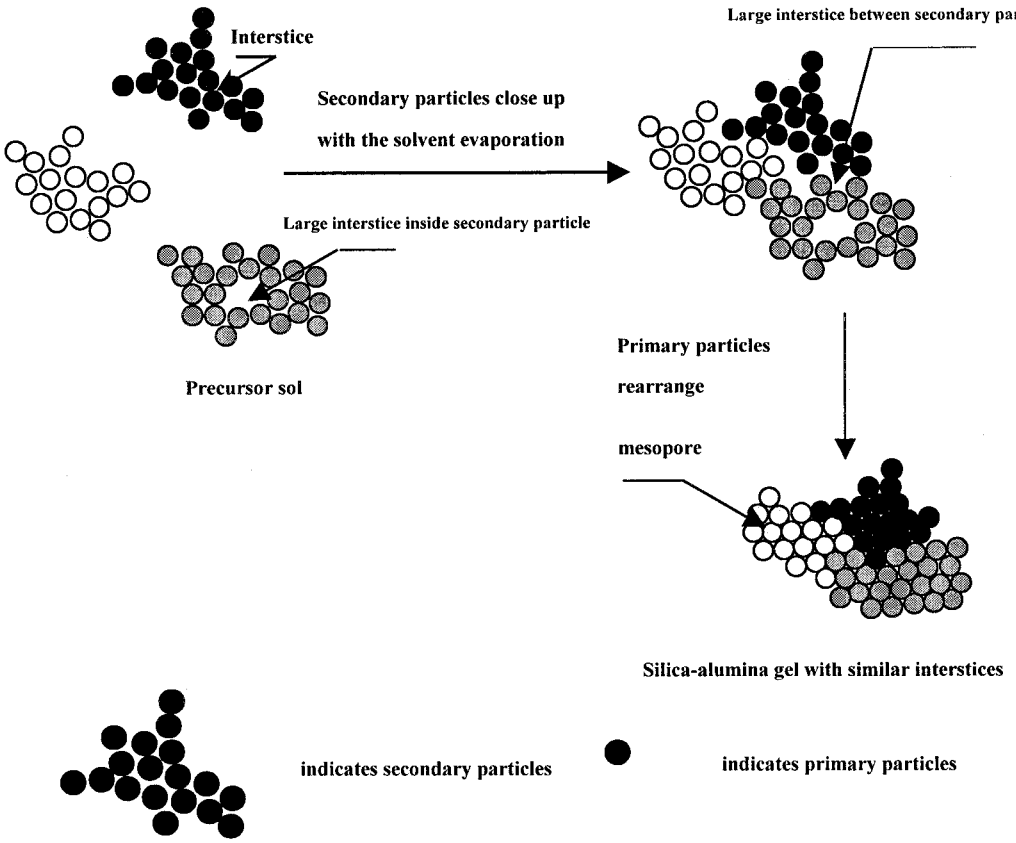

Figure 8. Schematic model proposed for the mesopore formation in these VSG materials.

the liquid will invade the pores with the greatest surface-to-volume ratio. This route will yield the greatest reduction in the energy of the system.[24] According to this concept, the liquid in the large interstices will flow to the small interstices. Due to the incompressibility of the solid and liquid, this liquid flow will force the primary particles to rearrange until all the interstices have similar sizes. Figure 8 illustrates this mesopore formation mechanism.

Because all the sols were dried under moderate conditions, the solvent was slowly evaporated and the drying time was long. This allows enough time for this rearrangement process to finish. After drying, most of the primary particles are regularly spaced and closely packed together, forming fluid-filled interstices with similar sizes, which are the precursors of the mesopores. With this mechanism, it is important to point out that the material's pore size distribution is determined by the size of the primary particles and their rearrangement process, but with no relationship to the secondary particles' size.

Although the data in Table 1 show that the precursor sols have large and different average particle diameters, they must have the same secondary particle structure as well as similarly sized primary particles like the VSG1 sol sample. The only difference is the size of these secondary particles. Therefore, according to the above mechanism and the related discussion, it is reasonable to propose that the synthesized materials have similar mesoporous distributions. This provides another proof confirming our suggestion that the primary particles rearrange themselves during the drying process to form regular packing. Had the rearrangement of the primary particles not taken place during the slow drying process, it would have been impossible to form the similar mesoporous distribution from those secondary particles with a different size distribution as shown in Figure 1B–D. Furthermore, it is important to indicate that if primary particles have broad size distribution, the similar sized interstices also would not be formed whether the rearrangement process occurred or not, due to the fact that packing of these primary particles will produce interstices with broad size distribution.

It is well-known that large particles are easily formed from Ostwald ripening. But in this study, we consider a better assumption would be that these large particles are formed by aggregation from primary particles rather than the Ostwald ripening. Otherwise, packing of those sol particles of hundred nanometer size would produce pore sizes greater than 40 nm.

3.4. Thermal Analysis Result. Figure 9 shows the typical TG and DTA patterns of the VSG4 gel sample. The TG curve can be divided into three regions defined by the accompanying weight loss. As can be seen from the TG curve, the weight loss between 40 and 150 °C (region I) is associated with a large endothermic peak in the DTA trace, corresponding to the desorption of physically adsorbed water. The region accompanying weight loss between 150 and 280 °C is defined as region II. An exothermic peak is observed at 250 °C in the DTA curve, which can be ascribed to the decomposition of NO_3^- anions. There is little weight loss occurring in the region above 280 °C (defined as region III) in the TG

(24) Brinker, C. J.; Scherer, G. W. *Sol–gel Science the physicals and Chemistry of Sol–gel Processing*; Academic Press Inc.: New York; Harcourt Brace Jovanovich: Orlando, FL, 1990; p 415.

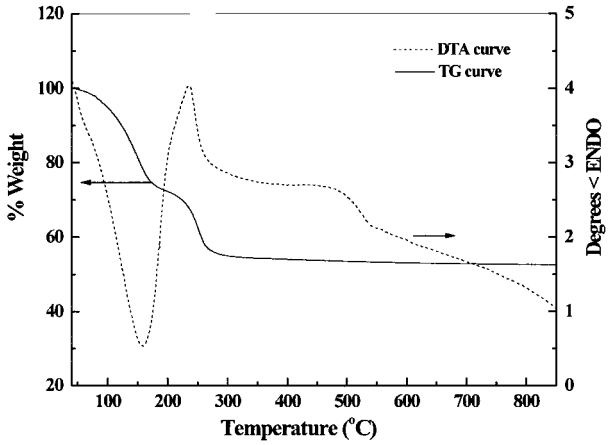

Figure 9. TG and DTA profiles of the VSG4 gel sample.

Table 3. Specific Surface Area and Pore Size Distribution of the VSG4 Sample Calcined at Different Temperatures

sample no.	heat treatment temp (°C)	specific surface area (m^2/g)	pore size distributn (nm)
VSG4	room temp	183.68	3.24−11.40
VSG4	150	379.76	3.15−10.20
VSG4	350	511.10	3.20−10.43
VSG4	550	542.99	2.12−10.61

curve. In this region, a small and broad endothermic peak can be observed in the DTA curve between 480 and 600 °C (the same feature is also observed in other samples). This peak may be attributed to the network shrinkage.

Table 3 summarizes the change of the specific surface area and pore size distribution of the VSG4 sample at increasing calcining temperature. According to our proposed mesopore formation mechanism, it is not surprising to note that the pore size distribution maintains a similar value during the heat treatment. This result indicates that the heat treatment has little influence on the pore size distribution. In Table 3, the specific surface area increases with increasing calcining temperature due to the removal of physically adsorbed water and NO_3^- anions. Usually, the most obvious physical change that occurs when an amorphous gel is heated above room temperature is shrinkage. The shrinkage accompanying weight loss in region I is small, but the shrinkage in region II is substantial.[25] In fact, the results shown in Table 3 indicate that the specific surface area increases in region II. Therefore, little shrinkage in the present materials takes place in this region when compared with the results reported in ref 25.

3.5. ^{27}Al and ^{29}Si Solid-State MAS NMR and Acidity Measurement Results. Figure 10A shows the ^{27}Al MAS NMR of the VSG solid samples. The broad peak at 52 ppm is due to aluminum atoms in tetrahedral $[AlO_4]^-$ environments, and the resonance at 0 ppm is from octahedrally coordinated aluminum. In addition to these two peaks, the samples also give a broad peak at 30 ppm assigned to 5-coordinate (AlO_5) aluminum.[26]

In Figure 10A, it is also seen that the proportion of tetrahedral aluminum decreases with a decrease in the Si/Al molar ratio. On the contrary, the proportion of 5-coordinated and octahedrally coordinated aluminum increases. These results are in agreement with the work reported by Hyun et al.,[27] who showed that an increase in the amount of the alumina component gradually changed the coordination number in silica−alumina from 4 to 6. In particular, both the peak position and the shape of the octahedrally coordinated aluminum change with the Si/Al molar ratio. It is seen that a symmetric peak at 0 ppm in the VSG4 spectrum changes to an asymmetric peak at 4.9 ppm in the VSG1 spectrum, as the Si/Al molar ratio decreases. This result seems to indicate that the content of alumina in the VSG materials largely affects the configuration of octahedrally coordinated aluminum.

Figure 10B shows the ^{29}Si MAS NMR spectra of these solid samples. The very large line widths observed in the spectra are indicative of the amorphous nature of the samples,[28] which is in good agreement with the XRD results. Furthermore, it is obvious that a broad shoulder appears only in the VSG1 sample's spectrum between −80 and −95 ppm. Figure 10C displays the related spectrum after deconvolution. It shows that two peaks appear at −85 and −92 ppm, which can be ascribed to the silicon atoms in the $Si(OAl)_4$ and $Si(OAl)_2(OSi)_2$ sites. Irwin reported that there were only $Si(OAl)_2$ species rather than $Si(OAl)_4$ species in the silica−alumina material prepared by the sol−gel method from alkoxides with a Si/Al molar ratio of 1. This indicates that a substantial portion of the aluminum is not a part of the oxide network, but is outside of it, perhaps acting to balance the network charge.[29] In contrast, it is certain that the amount of aluminum inside the network in the VSG1 sample is much higher than that inside the material prepared by Irwin with the same Si/Al molar ratio. Moreover, it also indicates that the silicon and aluminum in the VSG materials are more uniformly distributed and hence achieve better homogeneity even at a high alumina content. We believe this is one of the important advantages of our preparation method.

The densities of Brönsted and Lewis acid sites for these VSG materials are listed in Table 4. For reference, we have also included a typical commercial silica−alumina with 25% alumina content (CASA). As can be seen in Table 4, both Brönsted and Lewis acidities of the present materials are higher than those of CASA, except for the Brönsted acidity of the VSG1 sample. Thus, the VSG materials are suitable for many acid-catalyzed reactions. On the other hand, it was found that the number of Brönsted acid sites decreases in the order VSG4 > VSG3 > VSG2 > VSG1, in agreement with the decrease in the proportion of tetrahedrally coordinated aluminum, as shown in Figure 10A. However, the variation tendency of the Lewis acid sites is more complicated and needs further study.

(25) Brinker, C. J.; Scherer, G. W. *Sol−gel Science the physicals and Chemistry of Sol−gel Processing*; Academic Press Inc.: New York; Harcourt Brace Jovanovich: Orlando, FL, 1990; p 547.

(26) Dupree, R.; Farnan, I.; Forty, A. J.; Elmashri, S.; Bottyan, L. *J. Phys. Colloq.* **1985**, *C8*, 113.

(27) Hyun, S. H.; Yi, S. C.; Kim, S. G. *J. Mater. Sci. Lett.* **1996**, *15*, 1384.

(28) Fyfe, C. A.; Gobbi, G. C.; Putnis, A. *J. Am. Chem. Soc.* **1986**, *108*, 3218.

(29) Irwin, A. D.; Holmgren, J. S.; Jonas, J. *J. Mater. Sci.* **1988**, *23*, 2908.

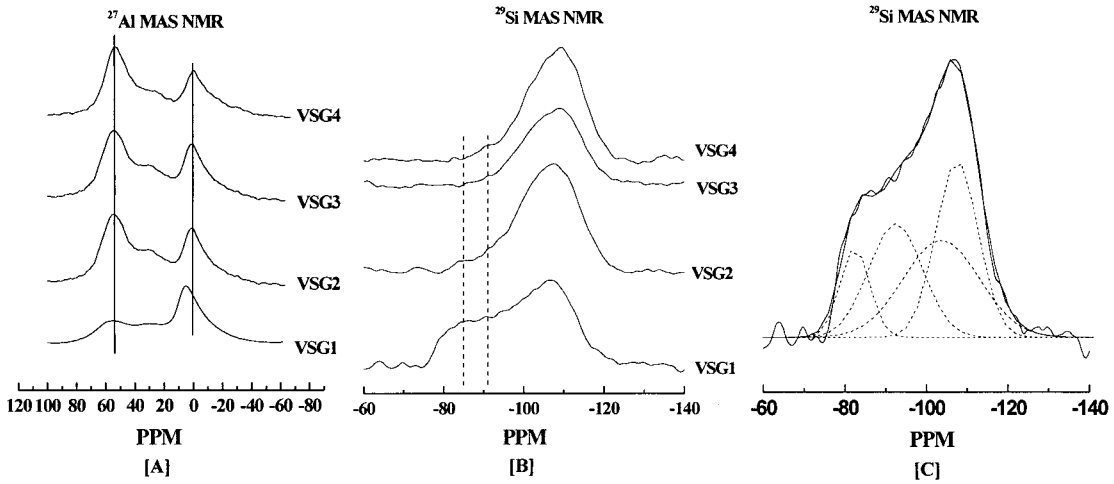

Figure 10. (A) ^{27}Al MAS NMR spectra of VSG solid samples with different Si/Al molar ratios. (B) ^{29}Si MAS NMR spectra of VSG solid samples with different Si/Al molar ratios. (C) ^{29}Si MAS NMR spectrum of the VSG1 solid sample deconvoluted by using the Gauss equation.

Table 4. Pyridine IR Data for Several VSG Samples with Different Si/Al Molar Ratios

sample no.	Si/Al molar ratio	desorptn temp (°C)	Brönsted acid site density (mmol/g) (1546 cm^{-1})[a]	Lewis acid site density (mmol/g) (1454 cm^{-1})[b]
VSG1	1	150	0.027	0.144
		250	0.019	0.083
		350	0.016	0.079
		450		0.040
VSG2	4	150	0.076	0.116
		250	0.047	0.080
		350	0.020	0.062
		450	0.005	0.054
VSG3	7	150	0.078	0.098
		250	0.055	0.079
		350	0.025	0.076
		450	0.020	0.069
VSG4	10	150	0.094	0.139
		250	0.056	0.099
		350	0.019	0.105
		450	0.009	0.098
CASA[c]		150	0.038	0.047
		250	0.025	0.046
		350	0.014	0.037
		450	0.006	0.036

[a] IR band attributed to pyridine adsorbed on Brönsted acid sites. [b] IR band attributed to pyridine adsorbed on aluminum Lewis acid sites. [c] Commercial silica−alumina catalyst [$Al_2O_3/(SiO_2 + Al_2O_3)$ = 25%] used at SINOPEC, People's Republic of China.

4. Conclusion

In the present study, without using any templates or PRAs, the developed synthesis method can prepare amorphous silica−alumina materials with various Si/Al molar ratios, narrow mesoporous distributions, and larger specific surface areas as compared to conventional methods. Inexpensive inorganic salts are used as raw materials, instead of using expensive and harmful alkoxides.

The results of N_2 sorption show that the synthesized materials have similar mesoporous distributions even if their precursor sols have different average particle diameters and Si/Al molar ratios. On the basis of the results of TEM, AFM, and nitrogen sorption, a formation mechanism of mesopores, proposing that the rearrangement process between similarly sized primary particles during drying determines the pore size distribution of the final materials, was also suggested. The mechanism can well explain the results shown in this study.

With the presented method, it is shown that the Si/Al molar ratio has great influence on the proportion of aluminum species as well as the configuration of octahedrally coordinated aluminum. The results also indicate that the distribution of silicon and aluminum in the present materials is more uniform and homogeneous than that in the mixed oxides prepared via the traditional sol−gel method at high alumina content. Moreover, the Brönsted acid sites of the synthesized materials decrease in the order VSG4 > VSG3 > VSG2 > VSG1, in agreement with the decrease in the proportion of tetrahedrally coordinated aluminum. Due to their acidic properties, the present materials are suitable for application in many acid-catalyzed reactions.

Acknowledgment. We are indebted to Prof. B. Delmon (Catalyse et Chimie des Université Catholique de Louvain, Belgium), Prof. Y. K. Kao (Department of Chemical Engineering, University of Cincinnati), and Prof. R. Xu (Key Laboratory of Inorganic Synthesis & Preparative Chemistry, Jilin University, People's Republic of China) for many valuable discussions. We are grateful to Ms. Xiumei Liu for acquiring the NMR spectra with DRX 400 and Prof. Jimmy C. Yu (Department of Chemistry, The Chinese University of Hong Kong) for improving the grammar of the manuscript. The financial support from the Chinese Academy of Sciences, the Research Institute of Petroleum Processing, SINOPEC, and the National Sciences Foundation of China is also acknowledged.

CM010270W